# An Improved Land-Surface Albedo Algorithm With DEM in Rugged Terrain

Jianguang Wen, Xiaojie Zhao, Qiang Liu, Yong Tang, and Baocheng Dou

***Abstract*—The influence of topography on land-surface bidirectional reflectance and albedo should be considered in rugged terrain. However, land-surface albedo algorithms neglect topographic effects, leading to errors in estimating the albedo in rugged terrain. This letter investigates the Angular Bin (AB) algorithm of land-surface albedo and shows that it should be improved when albedo is estimated in rugged terrain. The Terrain AB (TAB), an improved algorithm for albedo estimation with the AB algorithm and digital elevation model (DEM) data set, is presented in this letter. The accuracy and performance of the TAB algorithm was investigated by using the simulated DEM and Bidirectional Reflectance Function as well as the MODIS daily reflectance of the Heihe River Basin. The results show that the TAB algorithm has a better albedo estimation performance in rugged terrain and gives an acceptable accuracy.**

***Index Terms*—Angular Bin (AB) algorithm, land-surface albedo, rugged terrain, Terrain AB (TAB) algorithm, topographic effects.**

## I. Introduction

LAND-surface albedo is a primary controlling factor for surface energy balance and is thus a critical parameter affecting the Earth's climate [1]. Satellite remote sensing is the most practical way to estimate consistent data sets of land-surface albedo. The recent moderate- and low-resolution satellite remote sensing data, such as MODIS [2], MISR [3], and POLDER [4], are important for large- or global-scale albedo products.

Investigations of modeling land-surface albedo have shown that the spatial heterogeneity and complexity of land covers are the most challenging features [5], [6]. Rugged terrain, as a spatial heterogeneity factor, affects the estimation of land-surface albedo [7]–[9] in fine- and coarse-resolution data. However, the topographic effect in coarse-resolution data is often overlooked because the overall slope of coarse-resolution pixels is usually small and the adjacent reflectance is negligible. In practice, the topographic variation within one pixel is significant for coarse-resolution data in rugged terrains [10] and is treated as a modification to the Bidirectional Reflectance Distribution Function (BRDF) [11] due to the shadows and the tilt microarea surface within one pixel [12], [13].

Using a parametric factor which represents the effects of tilted area and mutual shadowing within a pixel is recommended as a necessary step in albedo estimation using a coarse-resolution remote sensing data in mountainous area [9]. However, this method requires a robust BRDF model to describe the land-surface reflectance anisotropy and to obtain the land-surface albedo.

In this letter, the Angular Bin (AB) algorithm [14] is selected as the base of BRDF/albedo algorithm. It is the main algorithm for Global LAnd Surface Satellite albedo production which had been globally distributed from December 2012. We formulate and demonstrate the performance of the Terrain AB (TAB) algorithm by synergistically using the AB algorithm and a parametric factor for land-surface albedo estimation from coarse-resolution satellite data in a rugged terrain. Moreover, it is necessary to specify that the formulation is to be at the spatial-resolution pixel of MODIS, AVHRR, and similar coarse-resolution sensors.

## II. Limitation of AB Algorithm for Rugged Terrain

A multivariant linear regression relationship is assumed between the surface broadband albedo and the surface bidirectional reflectance in MODIS visible and near-infrared spectral bands, which can be expressed as follows [14]:

$$a_{\mathrm{AB}} = c_0(\theta_s, \varphi_s, \theta_v, \varphi_v) + \sum_{i=1}^{n} c_i(\theta_s, \varphi_s, \theta_v, \varphi_v)\rho_i(\theta_s, \varphi_s, \theta_v, \varphi_v) \quad (1)$$

where $a_{\mathrm{AB}}$ represents the land-surface albedo [more specifically, the shortwave (0.3–3 $\mu$m) white-sky albedo or black-sky albedo (BSA) at a certain solar zenith angle]; $c_i(\theta_s, \varphi_s, \theta_v, \varphi_v)$ is the regression coefficient; and $\rho_i(\theta_s, \varphi_s, \theta_v, \varphi_v)$ is the surface directional reflectance at band $i$, which are all functions of solar/view angles.

The AB algorithm builds the linear regression relationship between the land-surface bidirectional reflectance on the MODIS bands and the broadband albedo. The algorithm has the advantages of simple computation, less input data requirements, and consideration of surface bidirectional and spectral characteristics [14]. The regression coefficients of the AB algorithm are estimated using the POLDER-BRDF data set, which covers global homogenous and flat land-surface types of the International Geosphere-Biosphere Program (IGBP). Therefore, the quality and representativeness of this training data set strongly influences the performance of the AB algorithm. Moreover, in

Manuscript received April 15, 2013; revised July 11, 2013; accepted August 26, 2013. Date of publication September 25, 2013; date of current version December 2, 2013. This work was supported in part by the Chinese Natural Science Foundation Project 41271368, 91025006, and 40901181, by the National Basic Research Program of China 2013CB733401, and by the National High Technology Research and Development Program of China under Grant 2012AA12A304.

The authors are with the State Key Laboratory of Remote Sensing Science, Institute of Remote Sensing and Digital Earth, Chinese Academy of Sciences, Beijing 100101, China (e-mail: wenjg@irsa.ac.cn; ppstoody@163.com; liuqiang@irsa.ac.cn; tangyong@irsa.ac.cn; dou3516@163.com).

Color versions of one or more of the figures in this paper are available online at http://ieeexplore.ieee.org.

Digital Object Identifier 10.1109/LGRS.2013.2280696

the case of the land-surface reflectance affected by the micro-area topography within coarse-resolution pixels, the regression coefficients are unsuitable.

## III. TAB Algorithm

An equivalent smooth surface directional reflectance $\rho(i_{\rm st}, \psi_{\rm st}, i_{\rm vt}, \psi_{\rm vt})$ is introduced for a virtual surface of the coarse-resolution pixel, which is assumed to be smooth so that there are no micro-area topography effects. $i_{\rm st}, \psi_{\rm st}, i_{\rm vt}, \psi_{\rm vt}$ are the equivalent relative solar zenith angle, relative solar azimuth angle, relative sensor zenith angle, and relative sensor azimuth angle, respectively [9], which can be estimated by the geometry of the sun/sensor and the fine-resolution digital elevation model (DEM) within a coarse-resolution pixel.

The modification reflectance by the micro-area topography $\rho(\theta_s, \varphi_s, \theta_v, \varphi_v)$ is written as a function of equivalent smooth surface directional reflectance $\rho(i_{\rm st}, \psi_{\rm st}, i_{\rm vt}, \psi_{\rm vt})$ and a parametric topographic factor $T(\mathrm{DEM}, \theta_s, \varphi_s, \theta_v, \varphi_v)$ [9]

$$\rho(\theta_s, \varphi_s, \theta_v, \varphi_v) = \rho(i_{\rm st}, \psi_{\rm st}, i_{\rm vt}, \psi_{\rm vt}) / T(\mathrm{DEM}, \theta_s, \varphi_s, \theta_v, \varphi_v). \quad (2)$$

According to (1), the albedo of the coarse-resolution pixels with geometry of $(i_{\rm st}, \psi_{\rm st}, i_{\rm vt}, \psi_{\rm vt})$ can be expressed as

$$a_{\rm TAB} = c_0(i_{\rm st}, \psi_{\rm st}, i_{\rm vt}, \psi_{\rm vt}) + \sum_{i=1}^{n} c_i(i_{\rm st}, \psi_{\rm st}, i_{\rm vt}, \psi_{\rm vt}) \rho_i(i_{\rm st}, \psi_{\rm st}, i_{\rm vt}, \psi_{\rm vt}) / T(\mathrm{DEM}, \theta_s, \varphi_s, \theta_v, \varphi_v). \quad (3)$$

Combining (2) and (3), the albedo of the coarse-resolution pixels in rugged terrain can be rewritten as

$$a_{\rm TAB} = c_0(i_{\rm st}, \psi_{\rm st}, i_{\rm vt}, \psi_{\rm vt}) + \sum_{i=1}^{n} c_i(i_{\rm st}, \psi_{\rm st}, i_{\rm vt}, \psi_{\rm vt}) \rho_i(\theta_s, \varphi_s, \theta_v, \varphi_v). \quad (4)$$

In this letter, this algorithm is defined as the TAB algorithm. One of the benefits of this algorithm is that the regression coefficient $c_i(i_{\rm st}, \psi_{\rm st}, i_{\rm vt}, \psi_{\rm vt})$ is from the same POLDER-BRDF data set and only the geometry of the sun–surface–sensor is changed. The regression coefficient reflects the characteristics of the reflectance $\rho(\theta_s, \varphi_s, \theta_v, \varphi_v)$ affected by topography. In (4), $c_i(i_{\rm st}, \psi_{\rm st}, i_{\rm vt}, \psi_{\rm vt})$ can be obtained from the lookup table through $i_{\rm st}, \psi_{\rm st}, i_{\rm vt}, \psi_{\rm vt}$.

## IV. Assessment of the TAB Algorithm's Performance

### A. Simulation of BRF and Land-Surface BSA

Nine simulated DEMs were generated with Gaussian height distributions to provide various roughness which indicates the degree of micro-area topographic effects. Each DEM was of $100 \times 100$ grid cells, and only the central part of the aforementioned DEMs was used to simulate a coarse-resolution pixel due to the ambiguous blocking of the micro-area in the edge of the DEM. Both grid cell and mean elevation are assumed 1 unit, and the standard error of elevation is 0.25 units. By appropriate vertical scaling using exaggeration and smoothing filter in the simulations, the DEMs with different slopes could be simulated. For this experiment, the unit is 30 m, the values of exaggeration in vertical elevation are 1, 10, and 20, and the Gaussian smoothing filters of extent are 11, 31, and 51 units [9]. The statistic mean slope is listed in Table I. To simplify the simulated coarse-resolution pixel, the DEM grid land cover is assumed vegetation and its anisotropy reflectance is extracted from the statistics of the MCD43B1 products. Table II shows the kernel coefficient of the MODIS seven-band statistical kernel coefficient, and the land type is vegetation.

According to the theory of geometric optics and radiosity, the radiative intensity of the coarse-resolution pixel can be expressed as the sum of the incremental radiative intensities over all the grid surfaces with different topography and mutual shadow [15]. Thus, the Bidirectional Reflectance Function (BRF) of the coarse-resolution pixel is simulated, and its BSA is calculated by integrating the BRF over all sensor view angles. The BSA has intense topographic effects because it depends on the solar relative incident angle [16]. Fig. 1 shows that the value of the BSA decreases with the steepness of the mean statistical slope. The steeper the slope, the greater the casting shadow, reducing the intensity of the sensor's reception.

TABLE I
DEM Mean Elevation and Mean Slope [9]

| filter | Exaggeration=1 | | Exaggeration=10 | | Exaggeration=20 | |
|---|---|---|---|---|---|---|
| | mean elevation (m) | mean slope (°) | mean elevation (m) | mean slope (°) | mean elevation (m) | mean slope (°) |
| 11 | 29.49 | 2.51 | 294.89 | 22.62 | 589.78 | 37.72 |
| 31 | 29.49 | 1.88 | 294.89 | 17.59 | 589.78 | 30.90 |
| 51 | 29.49 | 1.33 | 294.89 | 12.84 | 589.78 | 23.70 |

TABLE II
Statistical Kernel Coefficients of MODIS Band

| MODIS Bands | Volume kernel coefficients | Geometry kernel coefficients | Isotropic kernel coefficients |
|---|---|---|---|
| Band1 | 0.1372 | 0.0721 | 0.0279 |
| Band2 | 0.3213 | 0.2225 | 0.0416 |
| Band3 | 0.0695 | 0.0404 | 0.0128 |
| Band4 | 0.1172 | 0.0755 | 0.0216 |
| Band5 | 0.3625 | 0.2041 | 0.0559 |
| Band6 | 0.3151 | 0.1525 | 0.0582 |
| Band7 | 0.2160 | 0.0800 | 0.0487 |

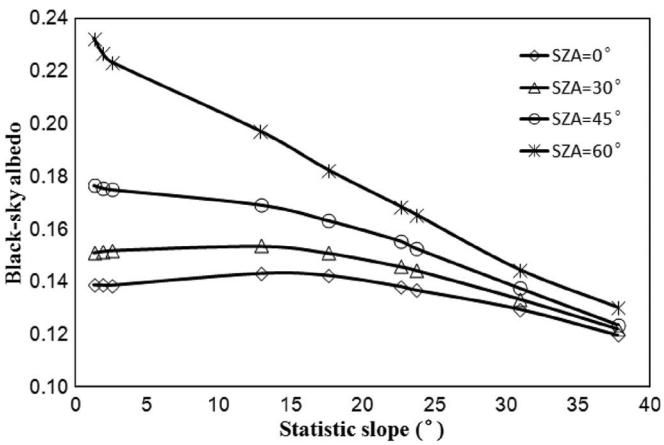


Fig. 1. BSA with different topographic effects.

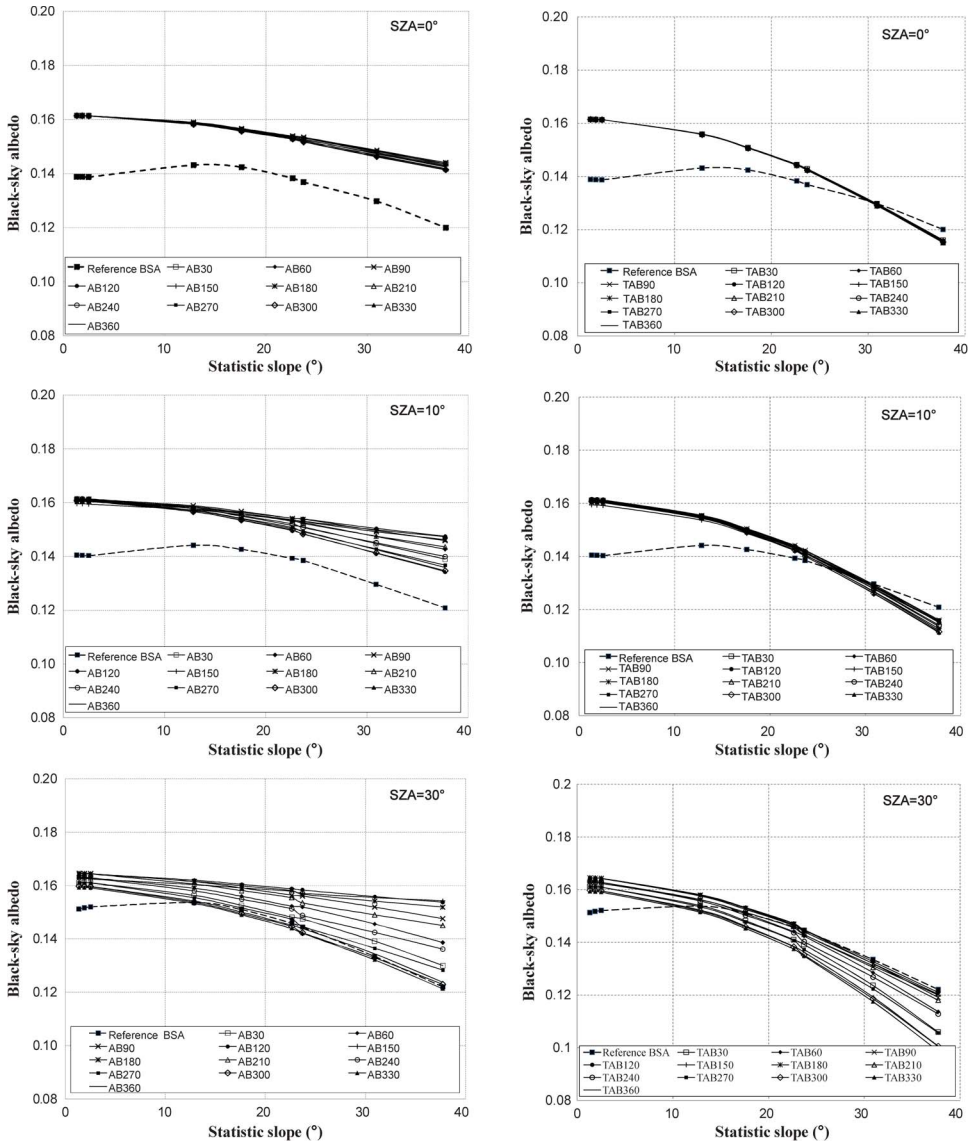


Fig. 2. BSA from the AB/TAB algorithm with different statistic mean slopes. Left figures are AB BSA, and right figures are TAB BSA. The two upper figures show the BSA of a sun zenith of 0° and an aspect of 150°, the two middle figures show the BSA of a sun zenith of 10° and an aspect of 150°, and the two bottom figures show the BSA of a sun zenith of 30° and an aspect of 150°. TAB/AB30 to TAB/AB360 indicate albedos calculated using different relative sensor azimuth angles, and the VZA is 20°.

### *B. Assessment of the TAB Algorithm's Performance*

The albedo estimated by the theory of radiosity is chosen as the reference albedo $a_0$. With (1) and (4), the deviation between the reference albedo $a_0$, the AB algorithm albedo $a_{\mathrm{AB}}$, and the TAB algorithm albedo $a_{\mathrm{TAB}}$ can be obtained. To alleviate the influence of the absolute value on the results of this analysis, the relative error instead of the absolute error with different relative azimuth angles is adopted to express the accuracy of the albedo estimation

$$\mathrm{RMSE}_{\mathrm{dAB}-0} = \sqrt{\sum_{k=1}^{n} \frac{(a_{\mathrm{ABk}} - a_0)^2}{n}} \tag{5}$$

$$\mathrm{RMSE}_{\mathrm{dTAB}-0} = \sqrt{\sum_{k=1}^{n} \frac{(a_{\mathrm{TABk}} - a_0)^2}{n}}. \tag{6}$$

where $k$ is the index of the sensor's azimuth angle. $\mathrm{RMSE}_{\mathrm{dAB}-0}$ denotes the relative error in albedo estimation caused by neglecting the micro-area topography between the AB algorithm and the reference albedo, and it shows the degree of the micro-area topographic effect on the albedo estimation. $\mathrm{RMSE}_{\mathrm{dTAB}-0}$ denotes the relative error in albedo estimation between the TAB algorithm albedo and the reference albedo, and it shows the precision of the TAB algorithm in coarse-resolution albedo estimation over the rugged terrain.

Fig. 2 shows the BSA results of the three algorithms at different statistical mean slopes and solar angles. The dotted line represents the BSA calculated by the radiosity algorithm as the reference; the solid line shows the AB and TAB BSA in terrains with different statistic slopes. A comparison between these albedos indicates that the resulting trends of both the AB and TAB algorithms are similar to the results of the radiosity algorithm. All the data in the figure confirm that when the mean

TABLE III
RMSE VALUES BETWEEN THE AB AND TAB BSAS RELATIVE TO THE REFERENCE BSA

| Mean slope | SZA=0° | | SZA=10° | | SZA=30° | |
|---|---|---|---|---|---|---|
| | AB | TAB | AB | TAB | AB | TAB |
| 1.33° | 0.023 | 0.023 | 0.020 | 0.020 | 0.011 | 0.011 |
| 1.88° | 0.023 | 0.023 | 0.020 | 0.020 | 0.011 | 0.011 |
| 2.51° | 0.023 | 0.023 | 0.020 | 0.020 | 0.010 | 0.010 |
| 12.85° | 0.015 | 0.013 | 0.014 | 0.011 | 0.005 | 0.003 |
| 17.59° | 0.014 | 0.008 | 0.013 | 0.007 | 0.006 | 0.003 |
| 22.62° | 0.015 | 0.006 | 0.013 | 0.004 | 0.008 | 0.005 |
| 23.70° | 0.016 | 0.006 | 0.013 | 0.003 | 0.008 | 0.005 |
| 30.90° | 0.018 | 0.001 | 0.017 | 0.002 | 0.014 | 0.009 |
| 37.72° | 0.023 | 0.005 | 0.021 | 0.007 | 0.020 | 0.014 |

slope increased, the TAB BSA gradually approached the value of the reference albedo.

The BSA of coarse-resolution pixels derived from the AB algorithm shows overestimation compared with the reference albedo range from the lower to higher mean slope, which means that the topographic effect on the AB albedo is not negligible for coarse-resolution pixels. Table III presents a comparison of the relative errors between the AB and TAB albedos relative to the reference albedo. The relative error of the AB albedo is larger, even exceeding 0.02 when the pixel has intense topographic effects.

The BSA of the coarse-resolution pixels derived from the TAB algorithm indicates the high deviation in the lower mean slope due to the TAB algorithm's invalidation for coarse-resolution pixels with less topography effects. The error is the same as in the AB algorithm, ranging from 0.011 to 0.023. There is a distinct adjustment in the high mean slope area. Lower errors can be found between the albedo from the TAB algorithm and from the radiosity algorithm. The relative error 0.023 is decreased to 0.005 when the mean slope is 37.32° and the solar zenith angle is 0°. Therefore, the TAB algorithm shows a good accuracy in coarse-resolution albedo estimation in rugged terrain.

## V. HEIHE RIVER BASIN LAND-SURFACE ALBEDO ESTIMATION

The Heihe River Basin, located in northwest China between 97.1° E − 102.0° E and 37.7° N − 42.7° N, covers an area of approximately 143 000 km$^2$. The Watershed Allied Telemetry Experimental Research (WATER) experiment of 2008 and the Heihe WATER (HiWATER) experiment of 2012 performed in the area show that the Heihe River Basin is an important base for the research of eco-hydro encounter logical characteristics [17]. Land-surface albedo is a fundamental parameter, and its estimation is effected by rugged terrain (Fig. 3).

Fig. 4 shows the BSA of the MCD43B3, the AB algorithm, and the TAB algorithm from 2011206 to 2011239 using the MODIS clear-sky daily reflectance product. It is clear that the albedo changed with the AB and TAB algorithms shows a smaller time scale (daily albedo) than the MCD43B3 algorithm (16-day composite albedo). The variation albedo is collected from four different statistic slopes within the MODIS pixel, which are flat terrain (1.81°), gentle rugged terrain (10.58°), and steep rugged terrain (20.81° and 35.68°), respectively.

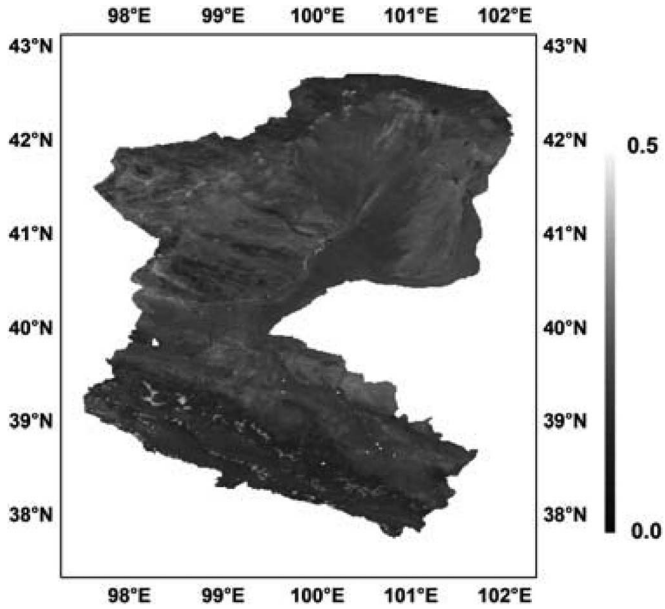


Fig. 3. BSA map of HiWATER area using TAB algorithm.

The albedos of the AB and TAB algorithm exhibit consistency at the flat and gentler rugged terrains, which can be considered as having less topographic effects. Moreover, compared with MCD43B3 albedo products, the bias is lower than 0.02. At the rugged terrain with steep slopes, there is great difference between the TAB albedo and the MCD43B3 and AB albedos because the latter two algorithms neglect the topographic effects on albedo. The absolute bias can be higher than 0.03. It is evident that topography intensively affects the albedo estimation although its absolute accuracy is difficult to evaluate in rugged terrain because of the limitation of *in situ* data.

## VI. SUMMARY

It is indicated that the topographic effects in albedo estimation are significant in rugged terrain. These effects are certainly an important error source, which is worth considering in land-surface albedo estimation. This letter has presented an effective algorithm for land-surface albedo estimation with DEM. The preliminary results show that the accuracy of the albedo estimation is acceptable.

Albedo estimation using the AB algorithm and the MCD43B3 product has been presented in this letter. Because of the topographic effects, these albedos do not reflect the actual albedo. The simulation results indicate that the deviation between the AB albedo and the reference albedo can be as large as 0.02 in rugged terrain. Using the TAB algorithm, the albedo presented in this letter shows a better agreement with the reference albedo in rugged terrain. The TAB algorithm in this letter is recommended as an improvement of the AB algorithm in albedo estimation from coarse-resolution remote sensing data in mountainous areas.

However, aside from the errors from the AB algorithm, neglecting the multiple scattering among the micro-areas of the rugged surface may explain the remaining inaccuracy in the TAB albedo in the simulated data set. In this letter, neglecting multiple scattering is regarded as an acceptable compromise

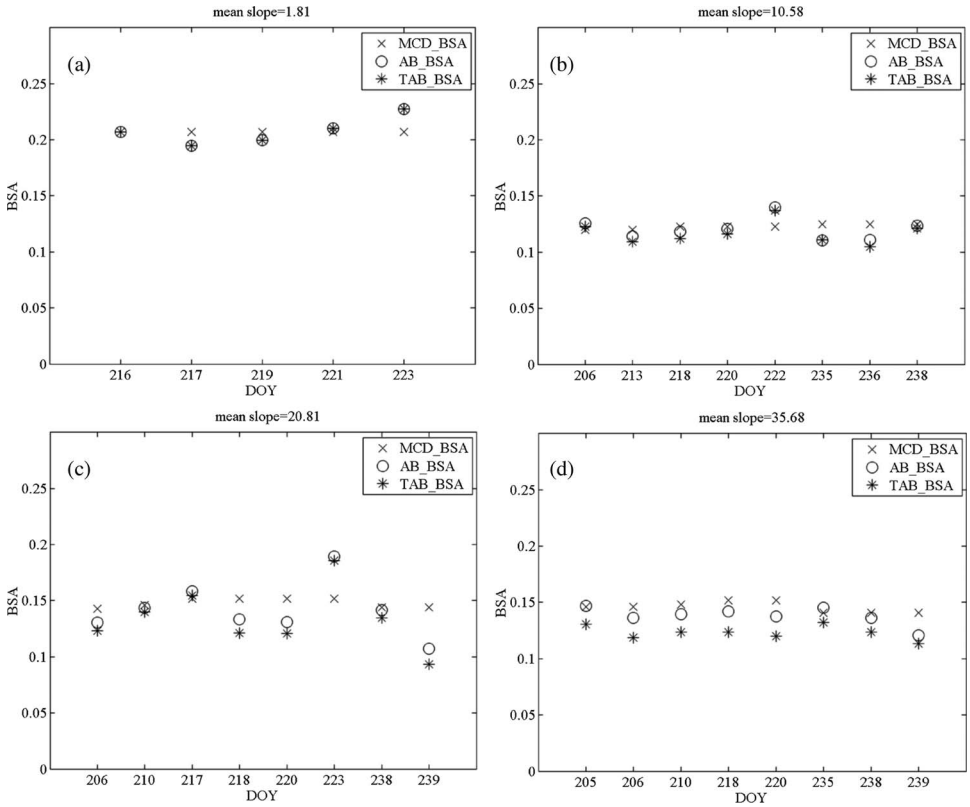


Fig. 4. BSA variation with different statistic slopes within the MODIS pixel: (a) Flat terrain, (b) gentle rugged terrain, and (c) and (d) steep rugged terrain.

between the accuracy and the model complexity due to the low multiple scattering in the main band of solar radiation. Additionally, the TAB algorithm's practical validation needs to be strengthened, although there is no effective way to obtain the coarse-resolution-pixel albedo in mountainous areas.

## REFERENCES


[1] R. E. Dickinson, "Land processes in climate models," *Remote Sens. Environ.*, vol. 55, no. 1, pp. 27–38, Jan. 1995.

[2] C. B. Schaaf, F. Gao, A. H. Strahler, W. Lucht, X. W. Li, T. Tsang, N. C. Strugnell, X. Y. Zhang, Y. F. Jin, J. P. Muller, P. Lewis, M. Barnsley, P. Hobson, M. Disney, G. Roberts, M. Dunderdale, C. Doll, R. P. d'Entremont, V. X. Hu, S. L. Liang, J. L. Privette, and D. Roy, "First operational BRDF, albedo and nadir reflectance products from MODIS," *Remote Sens. Environ.*, vol. 83, pp. 135–148, 2002.

[3] D. J. Diner, J. C. Beckert, T. H. Reilly, C. J. Bruegge, J. E. Conel, R. A. Kahn, J. V. Martonchik, T. P. Ackerman, R. Davies, S. A. W. Gerstl, H. R. Gordon, J. P. Muller, R. B. Myneni, P. J. Sellers, B. Pinty, and M. M. Verstraete, "Multi-angle imaging spectroradiometer (MISR) instrument description and experiment overview," *IEEE Trans. Geosci. Remote Sens.*, vol. 36, no. 4, pp. 1072–1087, Jul. 1998.

[4] M. Leroy and A. Lifermann, "The POLDER instrument onboard ADEOS: Scientific expectations and first results," *Adv. Space Res.*, vol. 25, no. 5, pp. 947–952, 2000.

[5] D. D. Baldocchi, T. Krebs, and M. Y. Leclerc, "Wet/dry Daisyworld: A conceptual tool for quantifying the spatial scaling of heterogeneous landscapes and its impact on the subgrid variability of energy fluxes," *Tellus B*, vol. 57, no. 3, pp. 175–188, Jul. 2005.

[6] Y. Ryu, S. Kang, S. K. Moon, and J. Kim, "Evaluation of land surface radiation balance derived from moderate resolution imaging spectroradiometer (MODIS) over complex terrain and heterogeneous landscape on clear sky days," *Agr. Forest Meteorol.*, vol. 148, no. 10, pp. 1538–1552, Sep. 2008.

[7] Y. F. Jin, C. B. Schaaf, C. E. Woodcock, F. Gao, A. H. Strahler, W. Lucht, S. L. Liang, and X. W. Li, "Consistency of MODIS surface bidirectional reflectance distribution function and albedo retrievals: 2. Validation," *J. Geophys. Res.*, vol. 108, no. D5, pp. 4159–4183, 2003.

[8] J. G. Salomon, C. B. Schaaf, A. H. Strahler, F. Gao, and Y. F. Jin, "Validation of the MODIS bidirectional reflectance distribution function and albedo retrievals using combined observations from the aqua and terra platforms," *IEEE Trans. Geosci. Remote Sens.*, vol. 44, no. 6, pp. 1555–1565, Jun. 2006.

[9] J. G. Wen, Q. Liu, Q. H. Liu, Q. Xiao, and X. W. Li, "Scale effect and scale correction of land-surface albedo in rugged terrain," *Int. J. Remote Sens.*, vol. 30, no. 20, pp. 5397–5420, 2009.

[10] S. L. Liang, *Quantitative Remote Sensing of Land Surface*. Hoboken, NJ, USA: Wiley, 2004, pp. 231–339.

[11] F. Q. Li, D. Jupp, M. Thankappan, L. Lymburner, N. Mueller, A. Lewis, and A. Held, "A physics-based atmospheric and BRDF correction for Landsat data over mountainous terrain," *Remote Sens. Environ.*, vol. 124, pp. 756–770, Sep. 2012.

[12] Y. G. Shkuratov, D. G. Stankevich, D. V. Petrov, P. C. Pinet, A. M. Cord, Y. H. Daydou, and S. S. Chevrel, "Interpreting photometry of regolith-like surfaces with different topographies: Shadowing and multiple scattering," *Icarus*, vol. 173, no. 1, pp. 3–15, Jan. 2005.

[13] H. Parviainen and K. Muinonen, "Rough-surface shadowing of self-affine random rough surfaces," *J. Quant. Spectrosc. Radiative Transf.*, vol. 106, no. 1–3, pp. 398–416, Jul./Aug. 2007.

[14] Y. Qu, Q. Liu, S. L. Liang, L. Z. Wang, N. F. Liu, and S. H. Liu, "Direct-estimation algorithm for mapping daily land-surface broadband albedo from MODIS data," *IEEE Trans. Geosci. Remote Sens.*, vol. 52, no. 2, pp. 907–919, Feb. 2014.

[15] I. Ashdown, *Radiosity: A Programmer's Perspective*. Hoboken, NJ: Wiley, 1994, pp. 34–54.

[16] J. M. Wang and F. Gao, "Discussion on the problems on land surface albedo retrieval by remote sensing data," *Remote Sens. Technol. Appl.*, vol. 19, no. 5, pp. 295–300, 2004.

[17] X. Li, G. D. Cheng, S. M. Liu, Q. Xiao, M. G. Ma, R. Jin, T. Che, Q. H. Liu, W. Z. Wang, Y. Qi, J. G. Wen, H. Y. Li, G. F. Zhu, J. W. Guo, Y. H. Ran, S. G. Wang, Z. L. Zhu, J. Zhou, X. L. Hu, and Z. W. Xu, "Heihe Watershed Allied Telemetry Experimental Research (HiWATER): Scientific objectives and experimental design," *Bull. Amer. Meteorol. Soc.*, vol. 94, pp. 1145–1160, 2013.